metals

MDPI

Article

Localized Perturbation Load Approach for Buckling Design of Thin-Walled Steel Cylindrical Shells under Partial Axial Compression

He Ma [1], Peng Jiao [1,2,*], Huangyang Xu [1], Xinshuang Li [1] and Zhiping Chen [1]

[1] College of Energy Engineering, Zhejiang University, Hangzhou 310027, China; mahe@zju.edu.cn (H.M.); 3190102950@zju.edu.cn (H.X.); 3190102019@zju.edu.cn (X.L.); zhiping@zju.edu.cn (Z.C.)
[2] School of Aeronautics and Astronautics, Zhejiang University, Hangzhou 310027, China
* Correspondence: jiaop@zju.edu.cn

Abstract: A thin-walled steel cylindrical shell is a common engineering structure that has an efficient load-carrying capacity. This structure is more easily subjected to partial axial compression loads in application, and buckling is the main failure mode. However, there are few available design methods for partial axially compressed steel cylindrical shells. Motivated by this, a design method called the localized perturbation load approach (LPLA) is proposed in this paper. The finite element framework for the application of LPLA is established. The location and number of perturbation loads are determined by considering the imperfection sensitivity and the buckling failure mode of partial axial compressed cylinders. A series of buckling experiments are carried out to validate the LPLA method. In addition, the reliability of LPLA for the design of cylindrical shells with different imperfection locations and dimensions is also verified. The results show that LPLA can give conservative and reliable lower-bound buckling loads. Therefore, LPLA can be used as a design method for thin-walled steel cylindrical shell structures under partial axial compression in actual engineering.

Keywords: thin-walled steel cylindrical shell; partial axial compression loads; buckling; lower-bound design; perturbation load; imperfection sensitivity

check for updates

Citation: Ma, H.; Jiao, P.; Xu, H.; Li, X.; Chen, Z. Localized Perturbation Load Approach for Buckling Design of Thin-Walled Steel Cylindrical Shells under Partial Axial Compression. *Metals* **2023**, *13*, 1539. https://doi.org/10.3390/met13091539

Received: 7 August 2023
Revised: 23 August 2023
Accepted: 28 August 2023
Published: 31 August 2023

Copyright: © 2023 by the authors. Licensee MDPI, Basel, Switzerland. This article is an open access article distributed under the terms and conditions of the Creative Commons Attribution (CC BY) license (https://creativecommons.org/licenses/by/4.0/).

1. Introduction

As a crucial engineering structure, the thin-walled steel cylindrical shell has obtained widespread application in most industrial fields. This structure tends to buckle when subjected to axial compression loads, and buckling failure is a critical concern in the design work of thin-walled cylindrical shell structures [1–6]. A large number of cylindrical shell buckling experiments have been carried out, and researchers have found that the experimentally observed buckling loads are far short of the theoretical predicted buckling loads of perfect shells [7,8]. Koiter [9] emphasized that the buckling loads of cylindrical shells are very sensitive to geometric imperfections. During the manufacture and transportation of steel cylindrical shell structures, geometric imperfections arise inevitably [10], which means a deviation between the actual shell shape and the perfect shape of the cylinder. Even small imperfections can significantly reduce the buckling load when the thin-walled cylindrical shell is under axial compression [11], so the influence of geometric imperfections should be carefully considered at the shell design stage.

The knockdown factor (KDF), the ratio of the buckling load of an actual imperfect cylindrical shell to the theoretical buckling load of a perfect shell, is defined to describe the gap between experimental results and theoretical results. In the 1960s, an empirical design guideline named NASA SP-8007 [12] was presented based on massive experimental results. This guideline provides a suggested lower-bound KDF and it is extensively used for shell preliminary design. Nevertheless, with the development of materials science and manufacturing technology, the NASA SP-8007 guideline has been proven to be

rather conservative [13–15], meaning that the related design may lead to structural redundancy and fund wastes. To avoid an overly conservative design, Arbocz and Babcock [16] presented a method to determine the KDF by considering the measured geometric imperfections from actual cylindrical shells. The calculated KDFs often agreed well with the test results. However, a serious problem is that the measured imperfections cannot be obtained in the shell design process before manufacturing. Thus, a cylindrical shell design method that does not rely on actually measured geometric imperfections is required.

The perturbation load approach is a type of deterministic analysis method based on numerical simulation. This approach triggers imperfections by exerting perturbation loads on the ideal cylindrical shell. The produced imperfections are treated as the "worst" case and the influence is greater than actual geometric imperfections, so the buckling load of the perturbated shell is calculated as the lower-bound design load [17]. Hühne et al. [18] proposed the single perturbation load approach (SPLA). In this approach, a single concentrated force is applied on the cylindrical shell as a perturbation load, causing a dent imperfection. The SPLA has been utilized by some researchers to design axially compressed cylindrical shells because of its convenience. However, Hao et al. [19] noted that the SPLA generally produces non-conservative KDFs because a single dent cannot envelop the effects of actual imperfections. Wagner et al. [20] indicated that the SPLA may provide a risky design buckling load for a cylindrical shell with an axisymmetric pre-buckling pattern. For the sake of improving the prediction method, Arbelo et al. [21] proposed the multiple perturbation load approach (MPLA). Multiple perturbation loads are adopted in the MPLA, rather than a single load. Jiao et al. [22] systematically investigated the effects of the perturbation load parameters on the MPLA, including the perturbation load number, magnitude and relative position. The MPLA has been verified as a promising method in predicting lower-bound buckling loads in comparison with the SPLA [23,24]. Furthermore, as a new type of MPLA, the worst multiple perturbation load approach (WMPLA) based on a surrogate model was proposed by Hao et al. [25] and Wang et al. [26] and then optimized by Tian et al. [27]. Their research indicates that the WMPLA can provide the design loads of axially compressed cylindrical shells with comparative accuracy.

However, the design methods of thin-walled cylindrical shell structures mentioned above are almost always applied in uniform axial compression loading conditions. In engineering, the actual loading case of steel or alloy cylindrical shells is distinctly more complicated [28,29]—for example, partial axial compression loads. The equipment set up on the top of a shell structure, such as the trestle piers installed on steel silos [30] or the ring cranes placed on top of nuclear containment shells [31], cause the partial distribution of axial compression loads, as shown in Figure 1. Moreover, discretely supported storage silos may bring about large reaction forces around the support column ends, which can make the cylindrical shell prone to buckling.

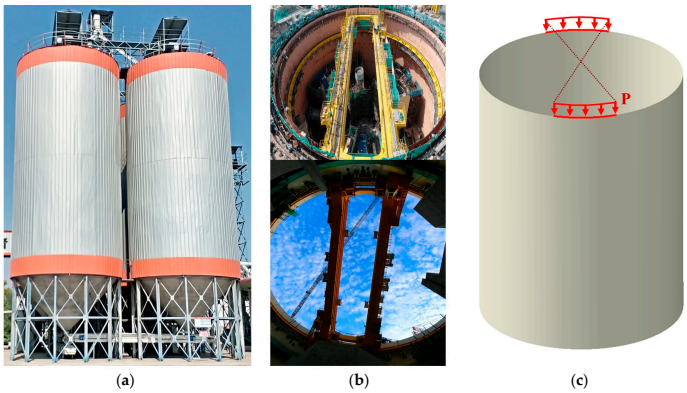


Figure 1. The partial axial compression loading condition: (**a**) trestle piers and discrete supports on cylindrical silos; (**b**) ring cranes on containment shells; (**c**) schematic diagram of partial axial load distribution.

Regarding the partial axial compression loading of thin-walled cylindrical shells, some studies have been carried out. Rotter et al. [32] studied the buckling behavior of a cylindrical shell with a locally high axial membrane stress distribution. The effects of structure geometrical parameters and imperfection amplitudes were discussed. Song et al. [33] carried out a series of numerical analyses of the load-carrying capacity of steel cylindrical shells, in which the partial axial loads were imposed on two loading regions at the shell end. An expression was presented by Khelil [34] to calculate the buckling loads of cylindrical shells under combined non-uniform axial loads and internal pressure. The dynamic stability of a simply supported composite cylindrical shell subjected to periodic partial loads was investigated by Dey and Ramachandra [35]. It was shown that for higher dynamic loads, the shell exhibited a chaotic behavior. In recent years, authors have performed a lot of experimental studies on thin-walled steel cylindrical shells under partial axial compression [36–38]. In our studies, over 40 steel cylindrical shell specimens with different loading cases were fabricated and tested. The buckling failure mechanism, load-carrying capacity and imperfection sensitivity of cylindrical shells were investigated in detail. Studies showed that the failure mode of steel cylindrical shells subjected to a small distribution of partial axial compression loads is local buckling, which is different from that in uniform axially compressed shells.

From the above research review, it can be found that the partial axial compression loads play a key role in the buckling of thin-walled cylindrical shells, which should be prudently considered in the shell design stage. However, to the best of our knowledge, there is still a lack of design methods for steel cylindrical shells under partial axial compression. Motivated by this, a new design method called the localized perturbation load approach (LPLA) to determine the design buckling loads of partial axially compressed cylindrical shells is proposed in this paper. The main innovation of this method is to consider the asymmetry of partial axially compressed cylindrical shells, and the perturbation loads are applied on the local area of the shell surface to cover the effects of geometrical imperfections. This method can serve as a safe design method for partial axially compressed cylindrical shell structures.

This paper is organized as follows. Section 2 presents the localized perturbation load approach. The FE modeling and the determination of the perturbation load parameters are introduced in detail. In Section 3, the localized perturbation load approach is validated by comparing the results with experimental studies as well as numerical studies of cylindrical shells with different imperfection locations or various dimensions. Finally, some important conclusions are summarized.

2. Localized Perturbation Load Approach (LPLA)

As a type of perturbation load approach, the basis of the localized perturbation load approach is to utilize the dent imperfections caused by perturbation loads to cover the adverse effects of actual geometric imperfections on shell buckling. Then, the lower-bound buckling loads of cylindrical shells can be obtained. However, the distribution of the partial axial compression loads breaks the symmetry of the cylindrical shells and changes the buckling behaviors [38]. Specifically, the buckling failure mode is local buckling, and the steel cylindrical shell is more sensitive to imperfections near the partial axial loading regions. Therefore, in the LPLA, the perturbation loads are applied on the local shell areas near the loading regions.

The flow diagram of the LPLA is shown in Figure 2 and a guide for the application of the LPLA in a finite element (FE) framework is also provided. The details of FE modeling as well as the determination of the perturbation load parameters, including location and number, are introduced in Sections 2.1–2.3.

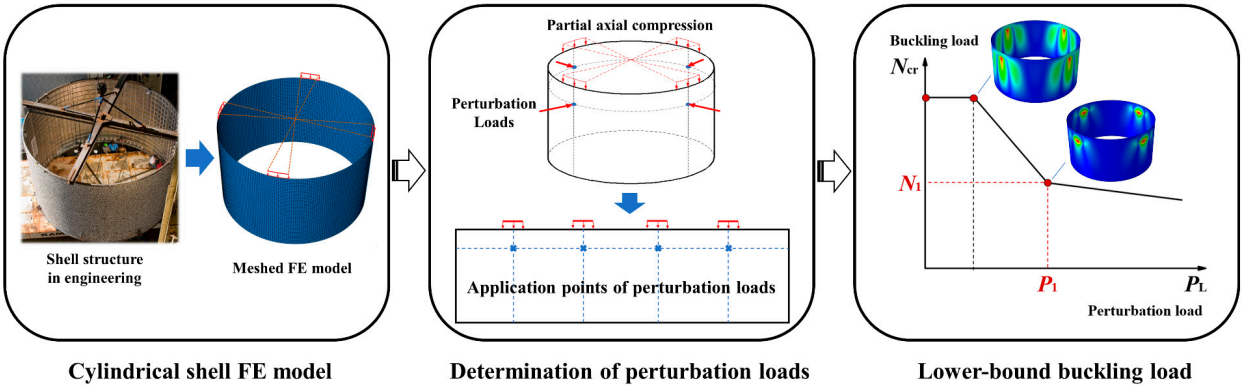


Figure 2. The localized perturbation load approach (LPLA).

1. Establishment of the cylindrical shell FE model with partial axial compression loading condition.
2. Determination of the location and number of perturbation loads according to the distribution of partial axial compression loads.
3. Calculation of the lower-bound buckling load as the design load of the cylindrical shell.

2.1. FE Modeling

All finite element models in the LPLA are established by the ABAQUS 6.14 software (SIMULIA Inc., Providence, RL, USA). The static analysis method with artificial damping is used for calculation. According to convergence studies, the value of the damping factor is determined to 1×10^{-6}. The dimensions and material parameters of the FE models are selected based on a reported study [38], as shown in Table 1. The ideal elastoplastic model is adopted as a material constitutive model. The cylinders are meshed by shell element S4R, which is a 4-node element with reduced integration. Moreover, the boundary conditions on both shell edges are clamped, but, at the top edge of the shell, the displacement is free in the axial direction for the application of partial axial loads. All nodes in the loading regions are linked to the reference point by coupling constraints, which act as rigid links to transmit axial compression loads. Then, an axial displacement U3 is applied on the reference point as the displacement-controlled axial compression load. Figure 3 shows the mesh and boundary conditions of the FE model.

Table 1. The parameters of cylindrical shell FE models.

Parameter	Value
Shell diameter, D (mm)	1000
Shell length, L (mm)	530
Shell thickness, t (mm)	1.2
Yield strength, R_{eL} (MPa)	149.4
Poisson's ratio, ν	0.3
Elastic modulus, E (GPa)	202.4
Damping factor	1×10^{-6}
Shell element type	S4R
Shell circumferential element number	400

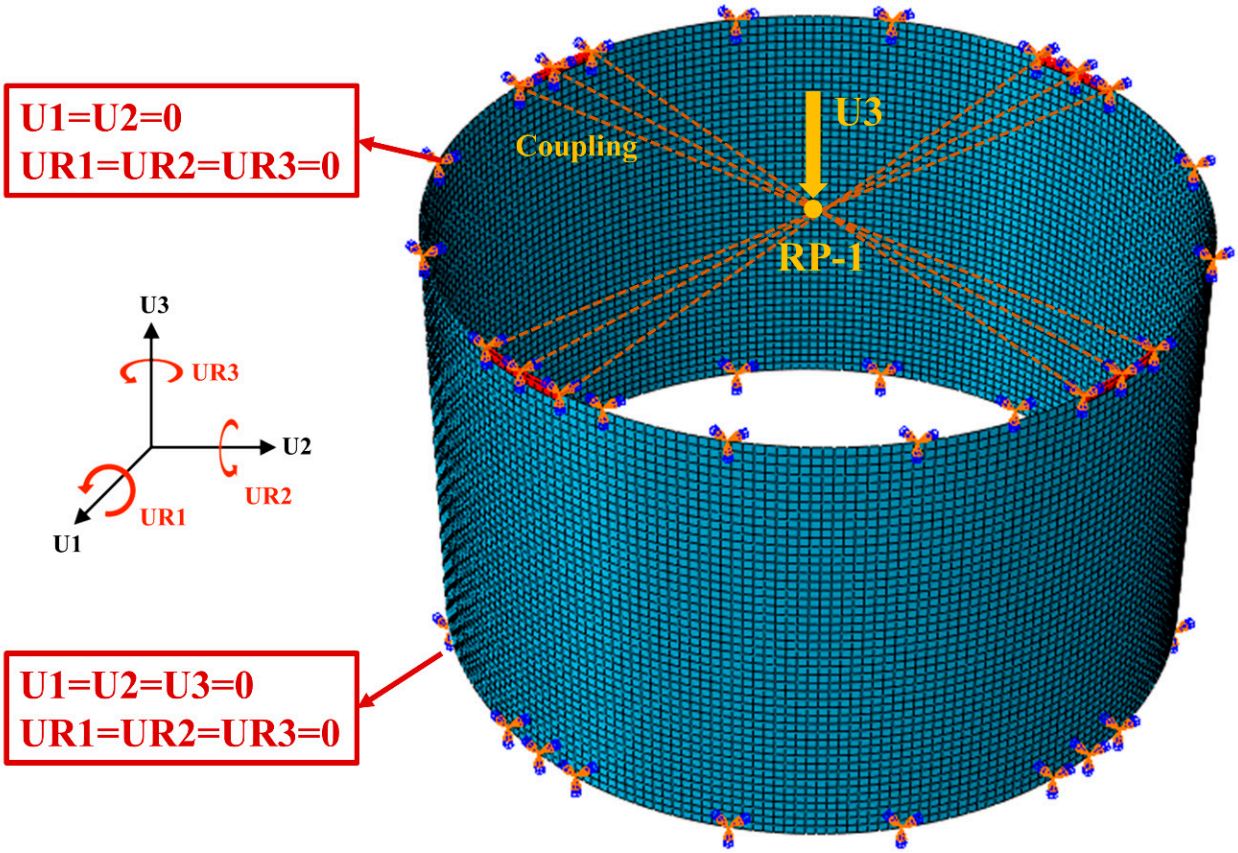


Figure 3. The mesh and boundary conditions of the FE model.

2.2. Determination of the Locations of Perturbation Loads

The perturbation load approach based on artificially inserted "worst" imperfections has been utilized to design a thin-walled cylindrical shell under uniform axial compression. Nonetheless, as previously mentioned, the buckling failure mode and imperfection sensitivity of cylindrical shells under partial axial compression are different from those in shells under uniform axial compression loads. Therefore, the locations of the perturbation loads in the LPLA need to be redetermined to cover the effect of geometric imperfections on shell buckling.

Figure 4 demonstrates the buckling deformation and stress distribution of cylindrical shells subjected to different levels of partial axial compression loads. For a more intuitive illustration, the contour plots are presented as 2D expanded diagrams, where U is the absolute value of radial deformation and S is the von Mises stress. It is worth noting that, in this paper, all loading regions of each shell are of the same size and are equally spaced apart from each other. This loading pattern fits most loading cases in actual engineering. We use the number and size (corresponding central angle) of the loading regions to refer to cylindrical shells under partial axial compression. For example, "$3 \times 10°$" means that the number of partial axial loading regions is 3, and, for each region, the central angle is 10°.

As shown in Figure 4, when the cylindrical shell has a small distribution of partial axial compression loads, the failure mode is local buckling. The cylindrical shell deforms greatly in the areas below the loading regions, while little deformation occurs in other areas far away from the loading regions. This is because the axial loads within a small scope have limited effects on the stress distribution of the cylindrical shell. Only the shell areas near the loading region have higher stress levels, and the material yield occurs first in these areas, accompanied by the extension of buckling deformation and a decrease in load-carrying capacity. However, when the distribution scope of the partial axial compression loads becomes larger, the shell failure mode changes to global buckling failure.

The yield areas extend and are finally connected together, and the buckling deformation gradually spreads over the whole circumference. The larger the distribution scope of the partial axial compression loads, the closer the shell buckling behavior is to the uniform axially compressed cylindrical shell. In this paper, only the design of cylindrical shells with local buckling failure mode is investigated. The size of each loading region is limited to smaller than 40°, and the total size of the loading regions on a cylindrical shell is smaller than 120°. This is in line with the loading cases of most engineering steel shell structures with discrete supports or equipment installation [30,31].

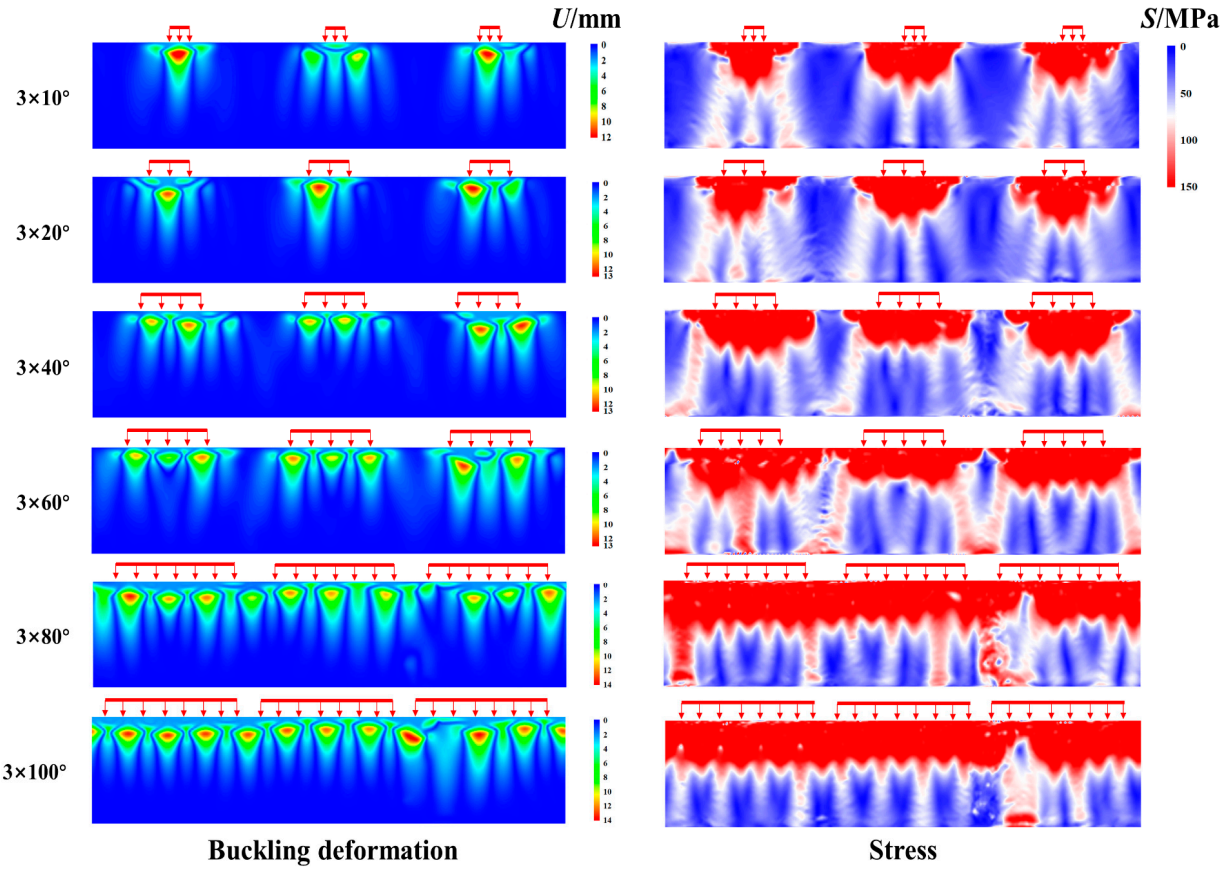


Figure 4. The buckling deformation and stress distribution of cylindrical shells subjected to different levels of partial axial compression loads.

Due to the asymmetry of the cylindrical shells under partial axial compression, changing the relative location of the geometric imperfections to the axial loads will change the shell buckling behaviors. The test specimen S-4-A is used to study the effect of the imperfection locations on the shell buckling behaviors. The distribution scope of the partial axial compression loads is 4 × 15°. The buckling tests of this series of specimens have been carried out in previous research [38], and the geometric imperfections are measured and imported into the shell FE model for calculation. The partial axial compression load is rotated around the axis within an angle α to change the relative locations of imperfections to axial loads. Figure 5 shows the buckling loads of shells with different imperfection locations, and the different locations of the loading regions are marked by red arcs in the top view of shells. $\alpha = 0°$ represents the real location of imperfections on the specimen. It can be found that changing the relative locations of geometric imperfections to partial axial compression loads causes a variation in the buckling load. When $\alpha = 80°$, the buckling load reaches the maximum value of 170.4 kN and the minimum value is 140.3 kN when $\alpha = 50°$.

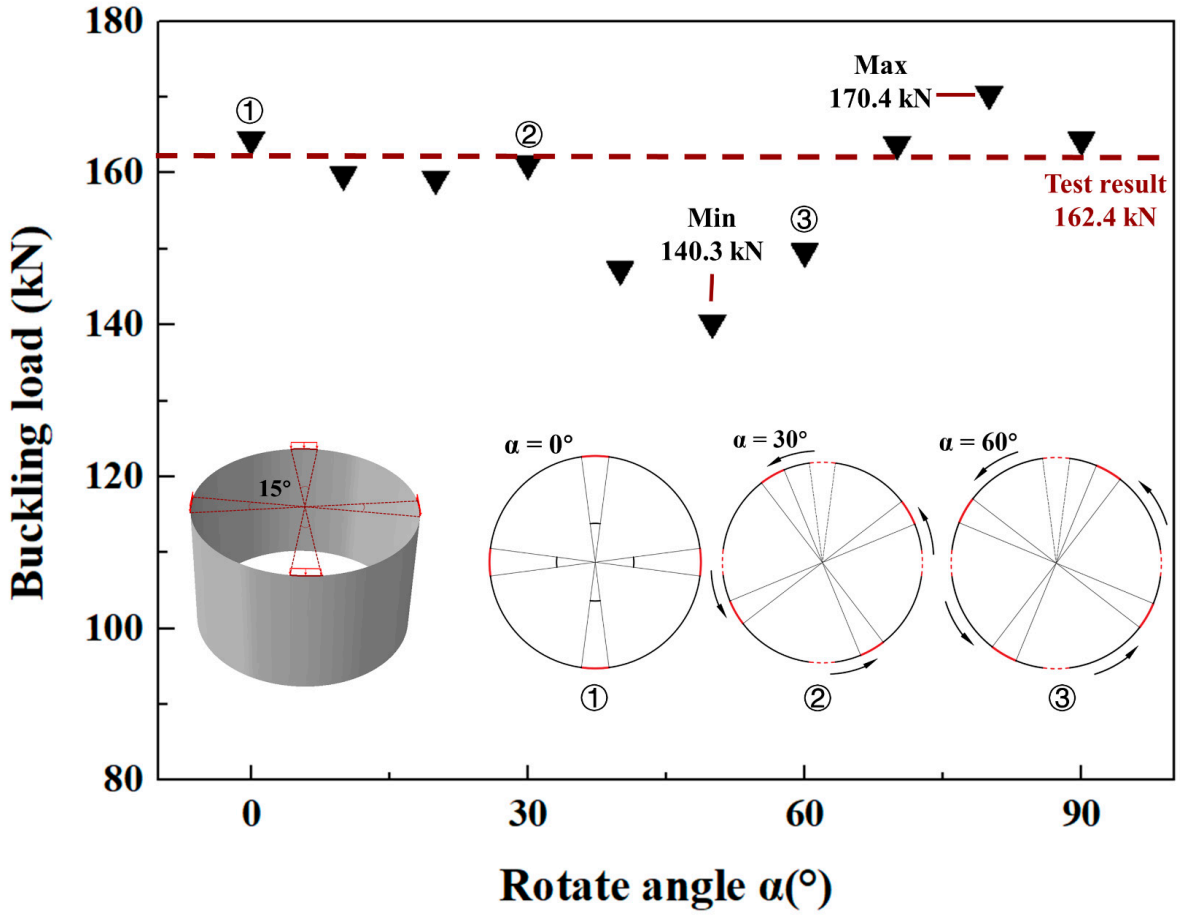


Figure 5. The buckling loads of cylindrical shells with different imperfection locations.

Figure 6 exhibits the buckling deformation of 4 × 15° partial axial compressed cylindrical shells with different imperfection locations in a critical buckling state and post-buckling state. $\alpha = 50°$ and $\alpha = 80°$ correspond to the minimum and maximum buckling loads. When the cylindrical shell structure is perfect and has no imperfections, its buckling deformation is symmetrical whether in the critical buckling state or post-buckling state. There is the same deformation below each axial loading region. Conversely, cylindrical shells with imperfections have asymmetrical deformation. The reason behind this phenomenon is that the randomly distributed geometric imperfections can weaken the load-carrying capacity of different areas of the shell to varying degrees. As shown in Figure 6a, the starting point of buckling deformation changes with the imperfection location. However, regardless of how the imperfection location changes, the shell buckling failure mode is always local buckling failure, and large deformation only appears below the loading regions. This indicates that the shell buckling mode is determined by the axial load distribution rather than the imperfection distribution. Furthermore, the cylindrical shells have different imperfection sensitivities at different shell areas when subjected to a small distribution of partial axial compression loads. The areas close to the axial loading regions are significantly affected by the imperfections, while areas far from the loading regions are insensitive to imperfections. This means that the perturbation loads need to be applied at the appropriate locations close to the loading regions, so that the dent imperfections can greatly reduce the load-carrying capacity of the cylindrical shell, thereby obtaining the lower-bound buckling load.

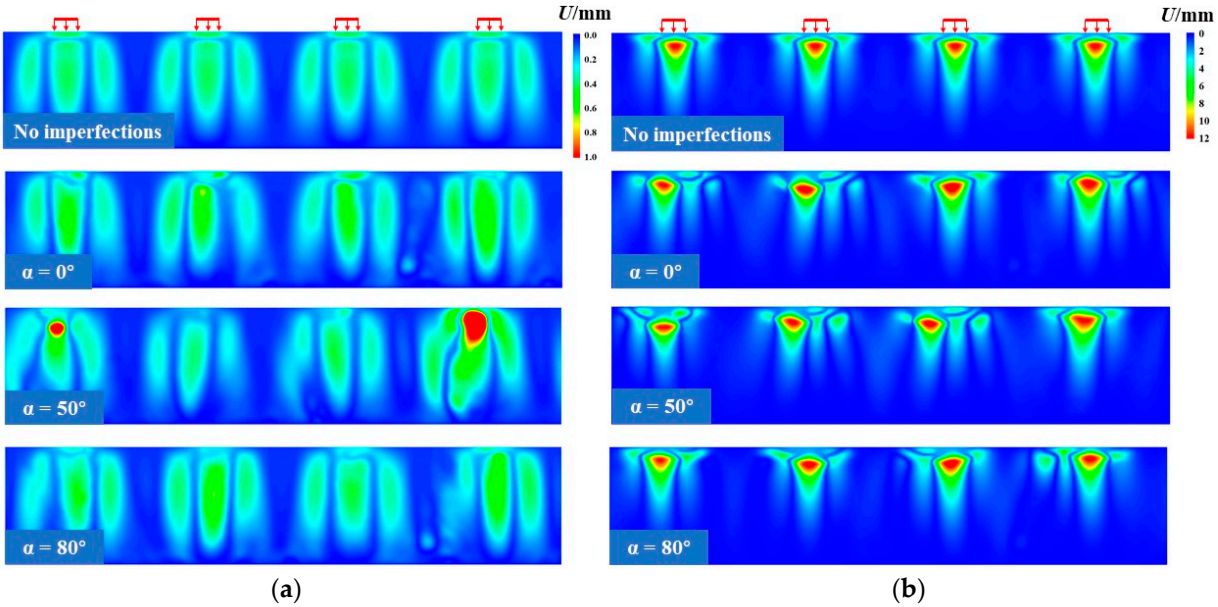


Figure 6. The buckling deformation of cylindrical shells with different imperfection locations: (**a**) critical buckling state; (**b**) post-buckling state.

Figure 7 shows the different locations of the perturbation load application points at the surface of a 4 × 15° partial axial compressed cylindrical shell. The shell can be divided into four identical parts, and each part corresponds to a 90° central angle with one 15° loading region. This figure shows the 3D schematic diagram and 2D unfolded diagram of a 90° shell part. The perturbation loads have the same locations in all four shell parts. For example, the perturbation load applied on point A1 represents that four equal loads are applied at the same A1 location in four shell parts. The vertical lines A and B, respectively, correspond to the locations below the middle and below the edge of a loading region, while vertical line C is located directly in the middle of two loading regions. The horizontal lines 1, 2 and 3 quarter the shell in the vertical direction. The nine intersections of the auxiliary lines are taken as the perturbation load application points to investigate the influence of different perturbation load locations on the shell buckling load.

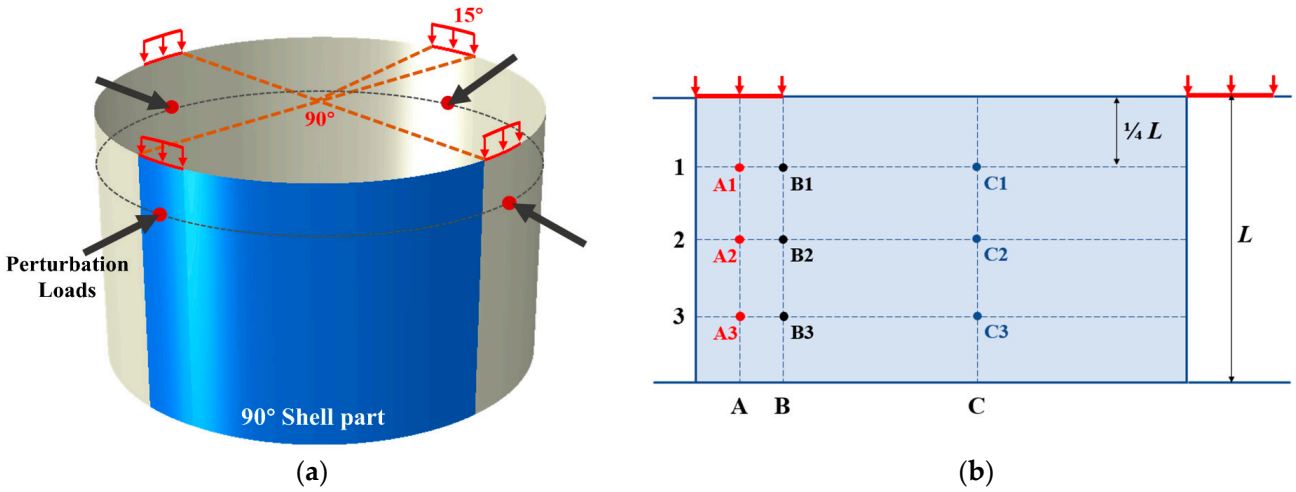


Figure 7. Different locations of perturbation load application points: (**a**) 3D schematic diagram of a cylindrical shell; (**b**) 2D unfolded diagram of a 90° shell part.

The relation curves of the shell buckling loads versus perturbation loads at each point are presented in Figure 8. The buckling load of a perfect cylindrical shell is also marked

with a horizonal line. It can be observed that these curves show three different types of trends. The curves A3, B3, C1, C2 and C3 coincide with the horizonal line. As the perturbation loads applied at these points increase, the buckling load is nearly constant. This phenomenon reflects that when the perturbation loads are applied far away from the partial axial compression loading regions, the obtained dent imperfections have little effect on shell buckling. In other words, the shell areas that are far away from the loading regions in the horizontal or vertical direction are insensitive to imperfections. This is consistent with the conclusion proposed above.

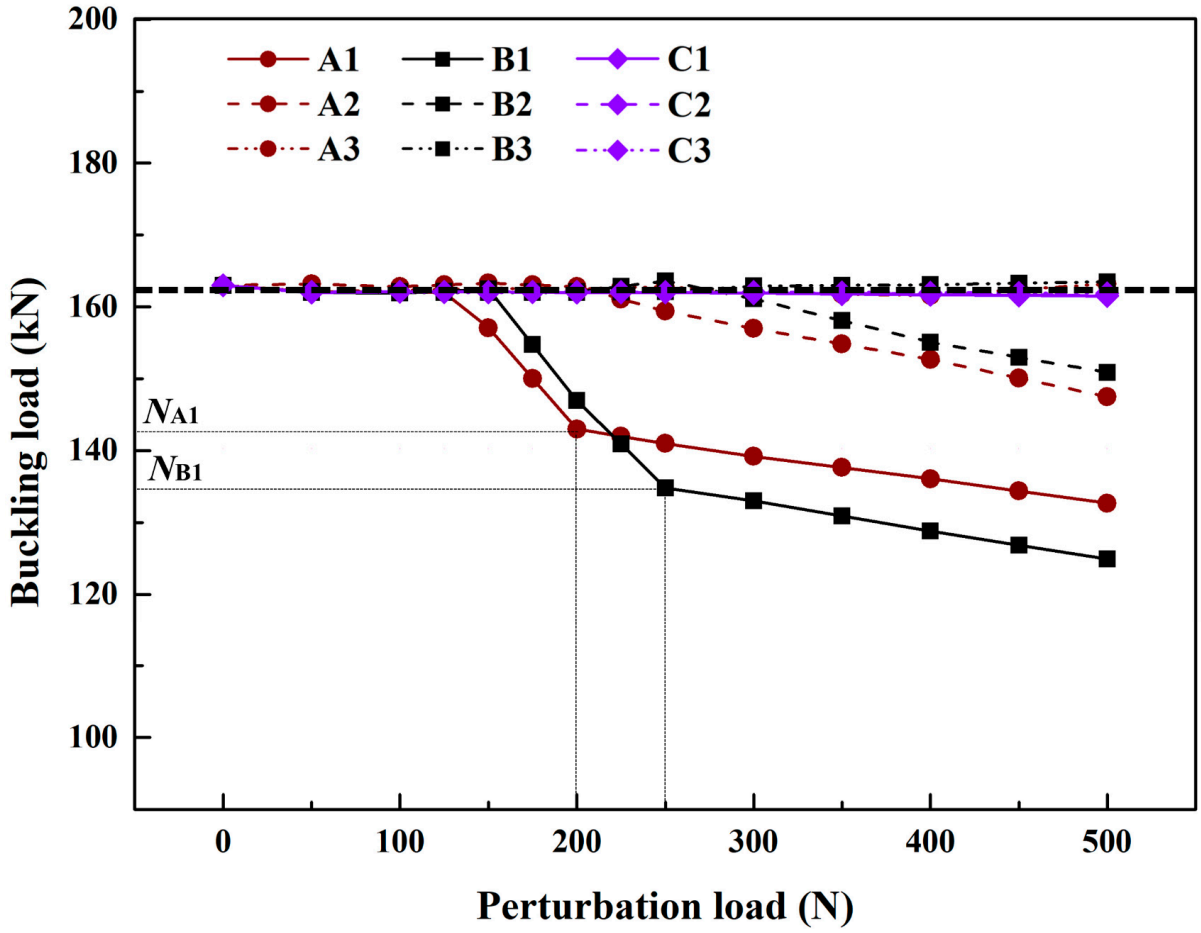


Figure 8. The relation curves of buckling load versus perturbation load under different perturbation load locations.

In contrast, when the perturbation load application points are near the loading regions, the buckling load changes greatly as the perturbation loads increase. The curves A2 and B2 show a different trend from A1 and B1. For curves A1 and B1, as the perturbation load gradually increases, the buckling load decreases rapidly until reaching the threshold value N_{A1} or N_{B1}. After the threshold, the buckling loads decrease slowly, although the perturbation load keeps increasing. In the perturbation load approach, the threshold value is defined as the lower-bound buckling load [18,22]. However, for curves A2 and B2, the buckling load begins to decrease continuously after the perturbation load reaches a certain value. It is difficult to obtain the lower-bound buckling load. Figure 9 shows the buckling deformation results of the $4 \times 15^{\circ}$ partial axial compressed steel cylindrical shell, including the experimental and numerical results of test specimen S-4-A, and the buckling deformation results of shells with different magnitudes and locations of perturbation loads. It can be found that the deformation result is more similar to the actual deformation when the perturbation loads are applied closer to the loading regions (A1 or B1). Therefore, compared to points A2 or B2, the perturbation loads applied on A1 or B1 can cover the

effects of imperfections on shell buckling better and can provide stable lower-bound buckling loads.

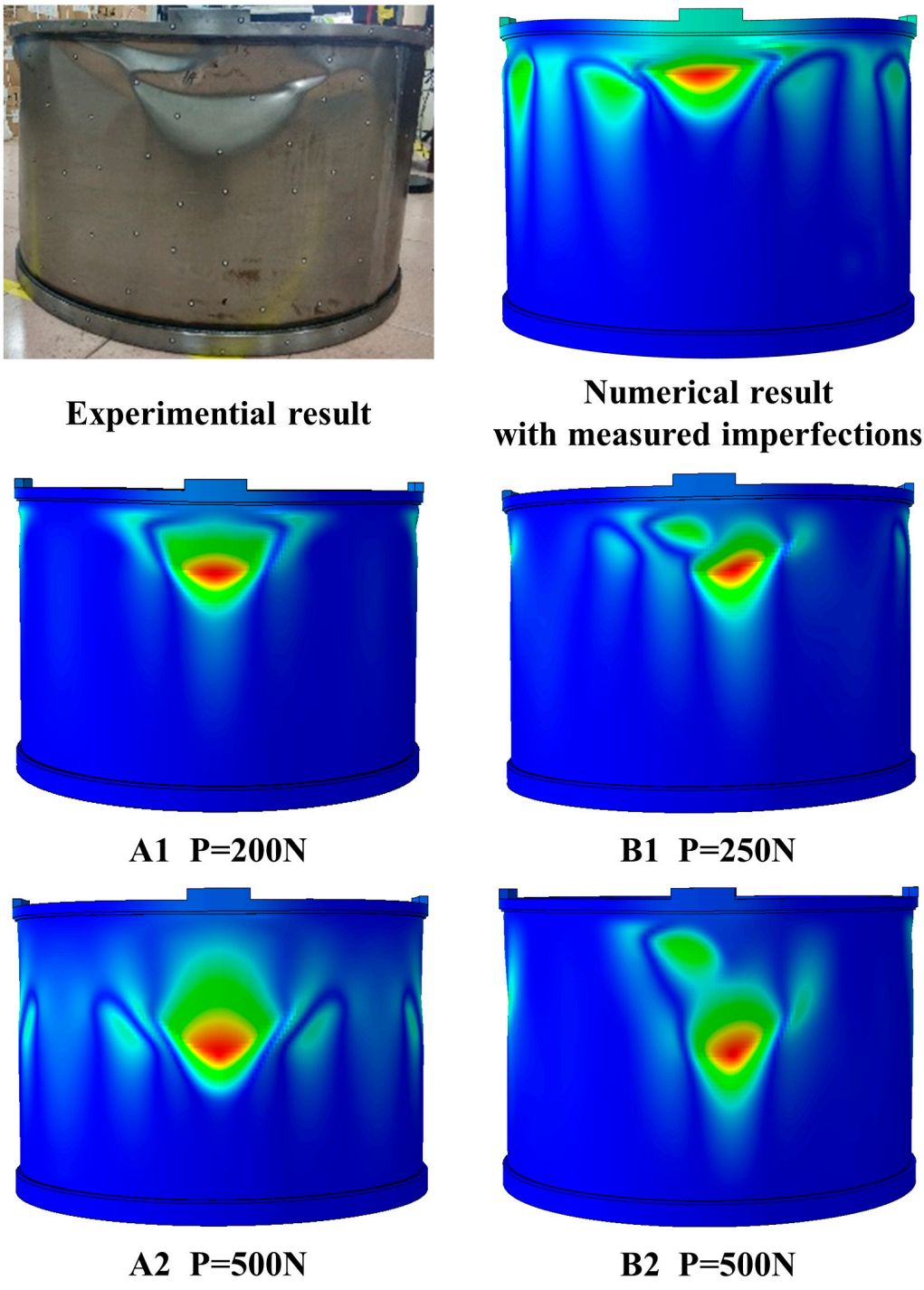


Figure 9. The buckling deformation results of steel cylindrical shells subjected to 4 × 15° partial axial compression loads.

To find the appropriate perturbation load application location to obtain a safe lower-bound buckling load, an investigation in a smaller distance range is carried out. As seen in Figure 7, when the distribution scope of the partial axial loads is small, the vertical lines A and B are very close. Thus, the relation curves of the shell buckling loads versus perturbation loads have the same trend when two equal-height perturbation loads are applied on the two lines—for example, A1 and B1, or A2 and B2. Therefore, only line A is considered here.

Several perturbation load application points located at a shorter path on line A are shown in Figure 10, and the vertical distance d between these points and the axial loading region is marked.

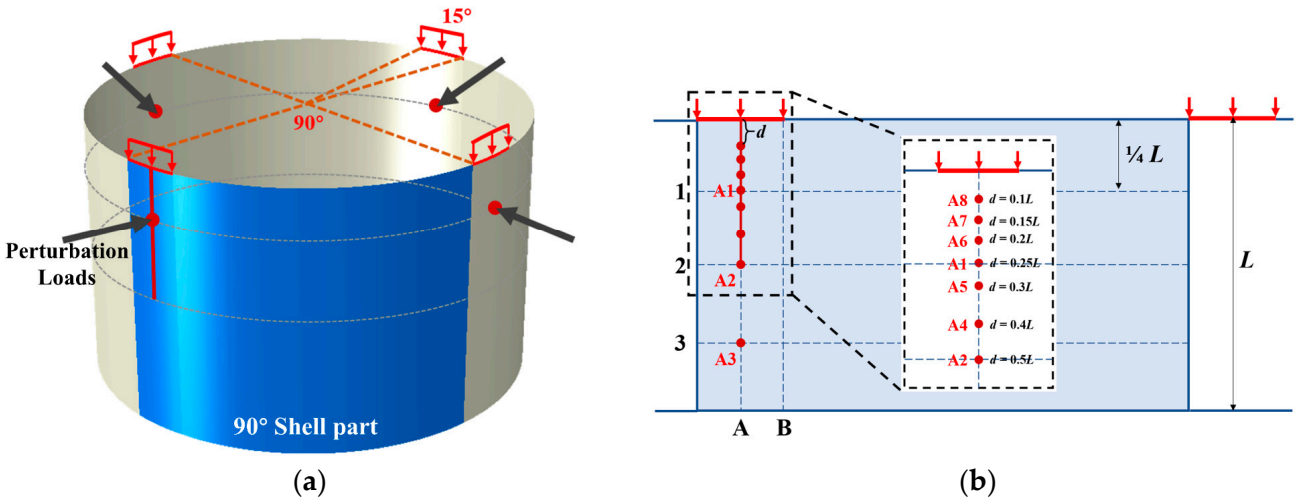


Figure 10. Different locations of perturbation load application points in a smaller range: (**a**) 3D schematic diagram of a cylindrical shell; (**b**) 2D unfolded diagram of a 90° shell part.

The relation curves of the shell buckling loads versus the perturbation loads of these points are presented in Figure 11. The lower-bound buckling loads obtained from these curves are all smaller than the test results. However, the effect of the imperfection locations should also be considered. The minimum results in Figure 5 are labeled as the riskiest case. From this perspective, when the perturbation loads are applied at points A6, A7 or A8, a safe lower-bound buckling load can be obtained. In addition, the curve A6 (d = 0.2L) has the most obvious threshold value and the value is not overly conservative.

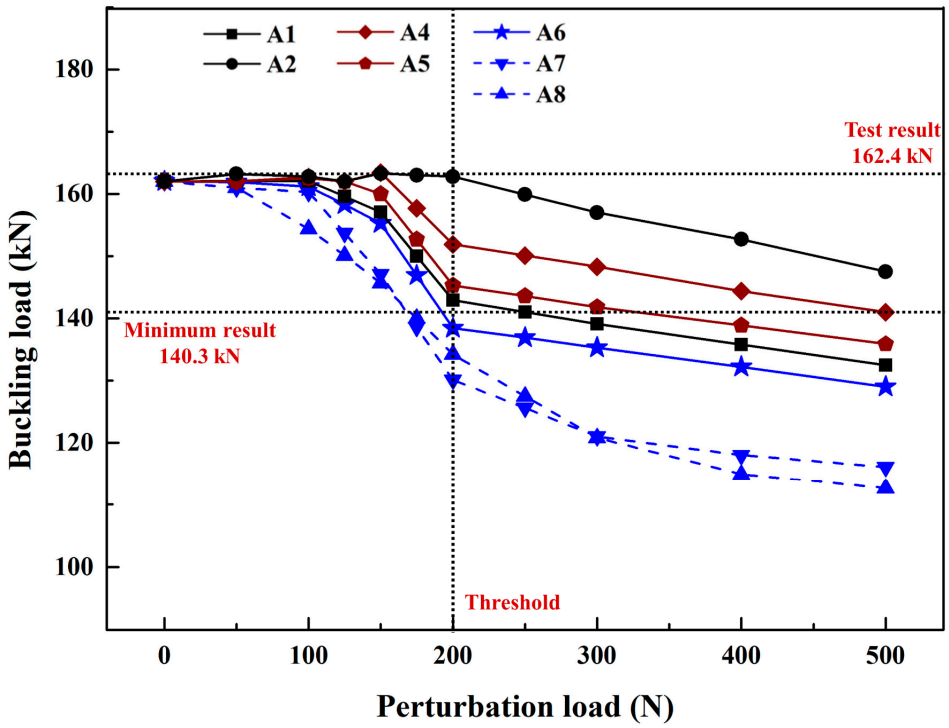


Figure 11. The relation curves of buckling load versus perturbation load of different perturbation load locations in a smaller range.

To summarize, in the LPLA, the perturbation loads are set right below the middle of the loading region, as with the location of line A. The vertical distance between the application point of the perturbation load and the axial loading region is the same as point A6, i.e., 0.2 times the shell length.

2.3. Determination of the Number of Perturbation Loads

As seen in Section 2.2, regardless of how the location of the perturbation loads changes, the perturbation load number is equal to the number of loading regions. Figures 12 and 13 show the relation curves of the buckling load versus perturbation load of cylindrical shells S-4-A and S-3-A with different numbers of perturbation loads. The distribution scope of the partial axial compression loads of S-3-A is $3 \times 20°$. The distribution of different numbers of perturbation loads is plotted in the top view of the cylindrical shell. The vertical distance from each perturbation load to the loading region is 0.2 times the shell length. In addition, the minimum buckling load 120.6 kN of S-3-A is marked in Figure 13, which is obtained by changing the relative location of the geometric imperfections to the axial loads.

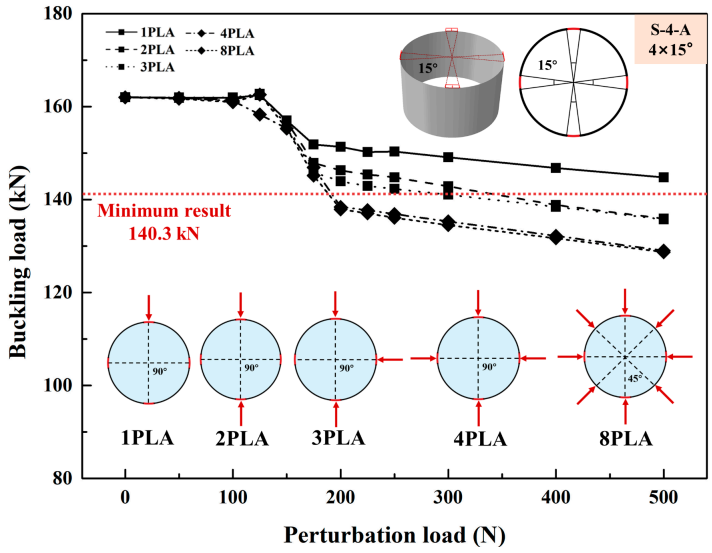


Figure 12. The relation curves of buckling load versus perturbation load of cylindrical shell S-4-A with different numbers of perturbation loads.

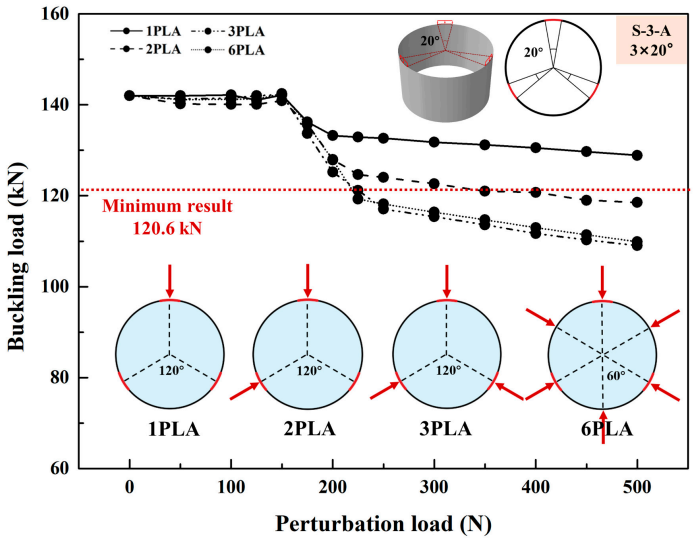


Figure 13. The relation curves of buckling load versus perturbation load of cylindrical shell S-3-A with different numbers of perturbation loads.

It can be found that the lower-bound buckling load changes with the number of perturbation loads. When the number of perturbation loads is less than the loading regions (1PLA/2PLA/3PLA of S-4-A, or 1PLA/2PLA of S-3-A), the lower-bound buckling load is greater than the minimum result. In other words, these cases provide non-conservative buckling loads. This is because, in these cases, there are no perturbation loads located below one or more loading regions, so the adverse effect of imperfections on shell buckling is not fully considered. Thus, the perturbation load approach gives higher buckling load results. However, when the number of perturbation loads is more than the loading regions (8PLA of S-4-A, or 6PLA of S-3-A), the conservative buckling load results can be obtained. The relation curves of the buckling load versus perturbation load basically coincide with the curves obtained from the cases when the number of perturbation loads is equal to the number of loading regions (4PLA of S-4-A, or 3PLA of S-3-A). This is due to the fact that the extra perturbation loads are applied away from the loading regions, which has little effect on shell buckling. Thus, in the LPLA, the appropriate number of perturbation loads is equal to the number of partial axial loading regions, and one perturbation load is applied below the middle of each loading region.

3. Validation of LPLA

3.1. Experimental Studies

3.1.1. Test Specimens and Platform

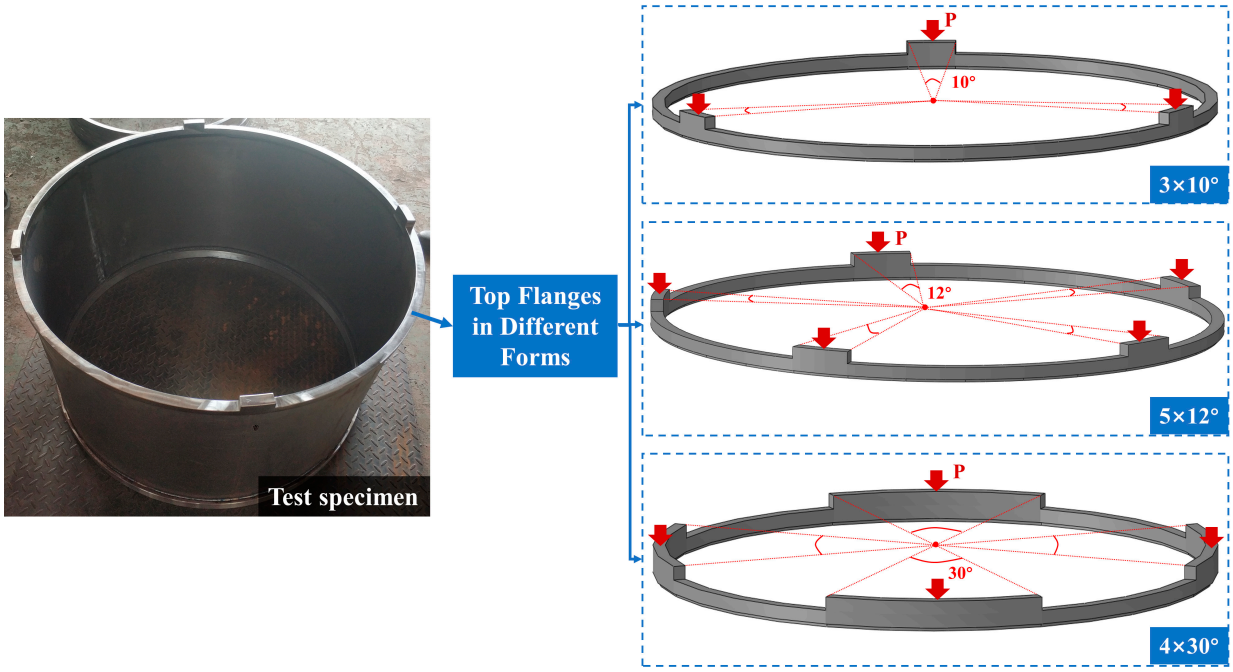
Buckling tests of thin-walled steel cylindrical shells under partial axial compression were carried out to validate the localized perturbation load approach. Different types of steel cylindrical shell test specimens were fabricated. The cylindrical shells were rolled by a DC01 steel sheet. Both ends of the shell were fully welded with specially designed flanges to ensure the transfer of partial axial loads and reduce the adverse boundary effect. Figure 14a shows some of the test specimen photos and top flange structures. The number and size of the prominent platforms on the top flange determine the distribution scope of the partial axial compression loads acting on the cylindrical shell.

Tensile tests were also conducted to determine the material properties of the test specimens. Three tensile coupons were fabricated with the same batch of shell steel sheets. The average values of Young's modulus E and yield strength R_{el} of the three coupons were taken as the mechanical material properties of the cylindrical shells. The Poisson's ratio v was directly taken as 0.3. These material properties are listed in Table 1 and are utilized for FE modeling in this paper.

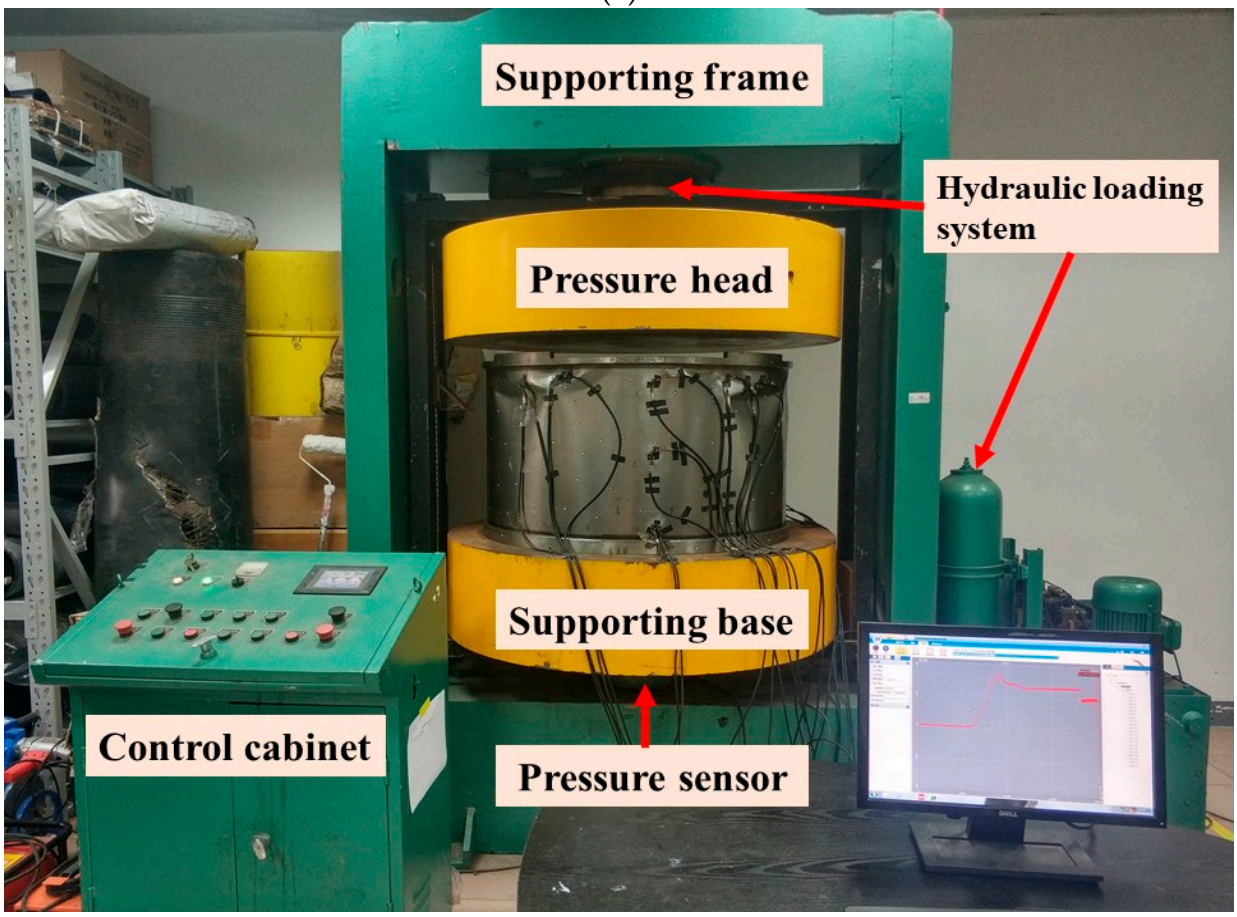
The buckling tests were performed on the axial compression buckling test platform displayed in Figure 14b. The hydraulic loading system could drive the pressure head to compress the specimen with a constant speed of 1 mm/min. Meanwhile, the axial compression signals could be acquired by the pressure sensor mounted on the bottom of the supporting base, so the axial load–time curve of each cylindrical shell specimen could be directly obtained. The movement mode of the pressure head could be switched by the electronic control cabinet. More detailed information about the buckling test platform can be found in Ref. [38].

3.1.2. Results and Comparisons

Figure 15 shows the test results of six steel cylindrical shells, including their buckling deformation and axial load–displacement curves. In addition, corresponding numerical studies were performed, and the results are also listed. The geometric imperfections of each specimen were measured by a Handy-Scan 3D laser scanner (CREAFORM Inc., Levis, QUC, Canada). In the numerical studies, the measured imperfections were imported into the cylindrical shell FE models by the inverse weighted interpolation method presented by Castro et al. [39]. It can be seen that the local buckling behavior could be well simulated in the numerical studies.



(**a**)



(**b**)

Figure 14. Test specimens and platform: (**a**) test specimens with different top flanges; (**b**) buckling test platform.

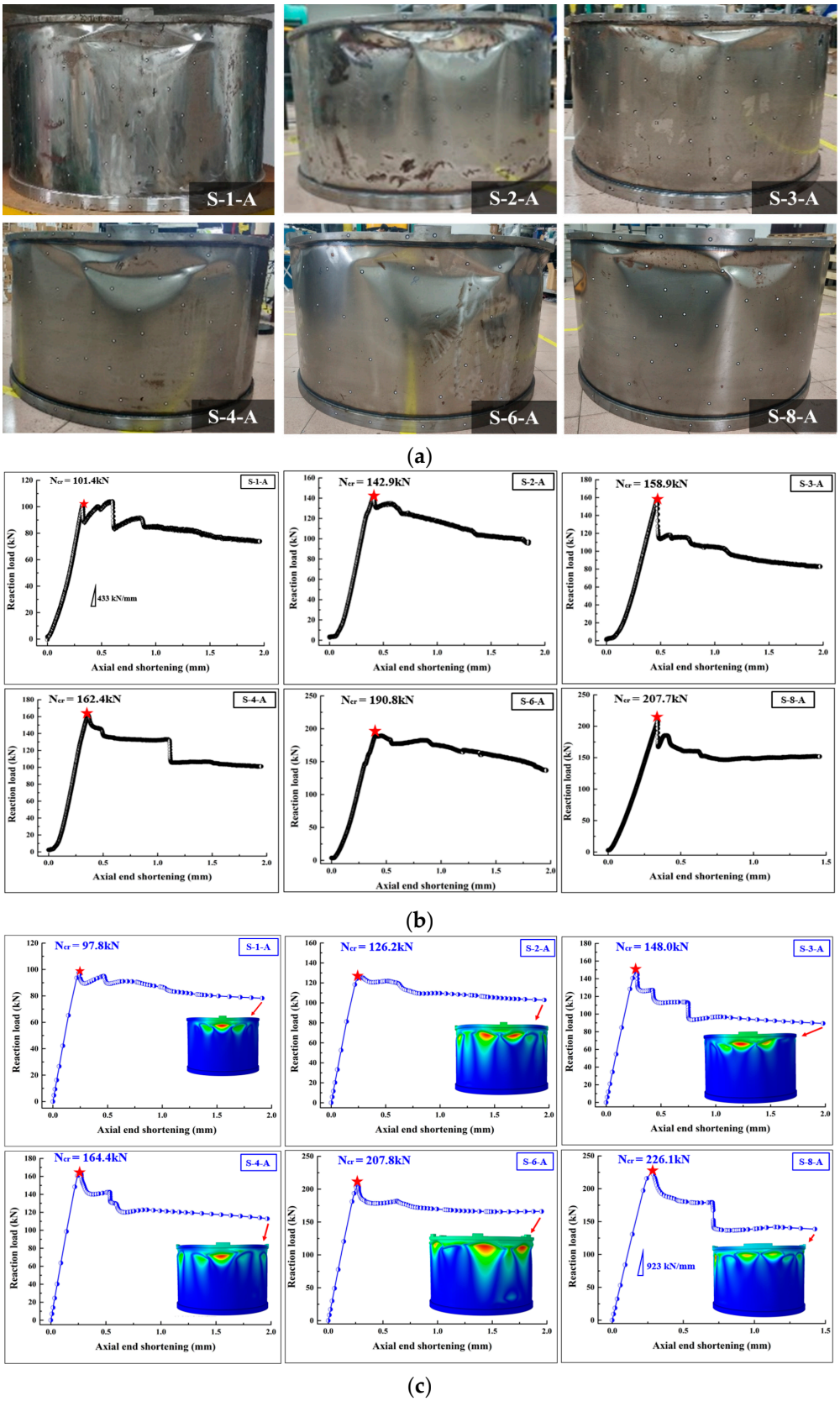


Figure 15. The experimental results and numerical results of test specimens: (**a**) the buckling deformation of test specimens; (**b**) the axial load–displacement curves of test specimens; (**c**) the numerical results of test specimens. The red stars represent the buckling loads which are marked in Figure 15c.

The buckling load results of all specimens obtained by the experimental studies (Exp) and numerical studies (Num) are listed in Table 2. The lower-bound buckling load of each steel cylindrical shell was calculated by the LPLA. The comparisons between the buckling loads obtained by the LPLA, buckling tests and numerical simulations are shown in Figure 16. The abscissa axis represents the experimental results, and the two vertical axes represent the numerical results and LPLA results. When a point is above the 45° dashed line, the ordinate value is greater than the abscissa value, meaning that the numerical/LPLA result is greater than the experimental result. Likewise, the points below the dashed line indicate that the numerical/LPLA results are less than the experimental results.

Table 2. Comparison of LPLA results and experimental results.

Cylindrical Shell	Loading Region	Experimental Results (Exp) (kN)	Numerical Results (Num) (kN)	LPLA Results (kN)	(LPLA-Exp)/Exp
S-1-A	3 × 10°	101.4	97.8	89.6	−11.64%
S-1-B	3 × 10°	117.4	107.6	89.6	−23.68%
S-2-A	4 × 7.5°	142.9	126.2	108.8	−23.86%
S-2-B	4 × 7.5°	131.9	131.1	108.8	−17.51%
S-3-A	3 × 20°	158.9	148.0	117.1	−26.31%
S-3-B	3 × 20°	123.7	139.6	117.1	−5.34%
S-4-A	4 × 15°	162.4	164.4	138.4	−14.78%
S-4-B	4 × 15°	171.3	159.3	138.4	−19.21%
S-6-A	6 × 10°	190.8	207.8	172.9	−9.38%
S-6-B	6 × 10°	204.3	207.6	172.9	−15.37%
S-7-A	3 × 40°	221.8	214.4	193.1	−12.94%
S-7-B	3 × 40°	218.3	198.5	193.1	−11.54%
S-8-A	4 × 30°	207.7	226.1	198.7	−4.33%
TS-1-1	2 × 15°	99.6	100.2	71.8	−27.91%
TS-1-2	2 × 15°	96.6	102.7	71.8	−25.67%
TS-1-3	2 × 15°	86.7	95.9	71.8	−17.19%
TS-2-1	2 × 15°	139.1	151.8	110.5	−20.56%
TS-2-2	2 × 15°	138.9	145.4	110.5	−20.45%
TS-2-3	2 × 15°	124.7	135.1	110.5	−11.39%

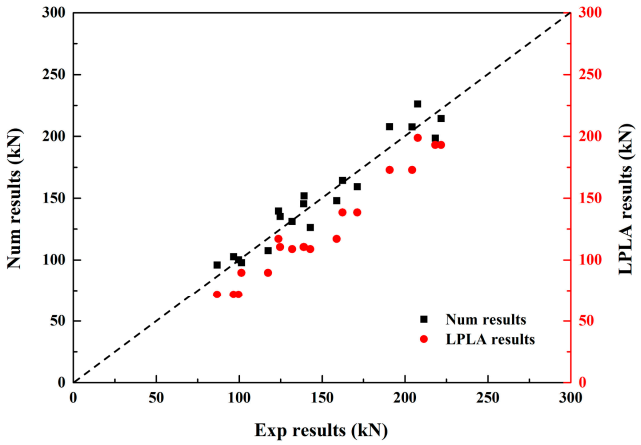


Figure 16. Comparison of LPLA results, Num results and Exp results.

It can be seen from the comparison that the numerical results are closer to the experimental results than the LPLA results. The reason is that the numerical simulations consider the real imperfections on steel cylindrical shells. It is worth noting that there are some deviations between the Exp results and Num results, which depend on the manufacturing accuracy of the test specimens. From Table 2, the deviations between the experimental results and numerical results are mostly less than 10%, so the accuracy of the FE models proposed in this paper is acceptable.

As mentioned above, the measured imperfections cannot be obtained in the shell design process before manufacturing. Therefore, a numerical simulation based on measured imperfections cannot achieve the appropriate design load of the cylindrical shells under partial axial compression. All LPLA results are lower than the experimental results. The maximum deviation between the two results is −27.91%, while the minimum deviation is −4.33%. This indicates that the LPLA can provide safe buckling loads for these steel cylindrical shells and can be utilized as a lower-bound design method for shell buckling.

3.2. Numerical Studies with Different Imperfection Locations

As mentioned in Section 2.2, the distribution of partial axial compression loads makes the cylindrical shell asymmetrical. The variation in the relative location of geometric imperfections to axial loads may change the load-carrying capacity of shells. Figure 17 shows the buckling loads of six steel cylindrical shells with different relative locations of the geometric imperfections and different distributions of partial axial compression loads. Similarly, the change in the relative location is represented by the rotation angle α of the partial axial compression. Table 3 compares the minimum buckling loads of six shells with different imperfection locations with the LPLA results.

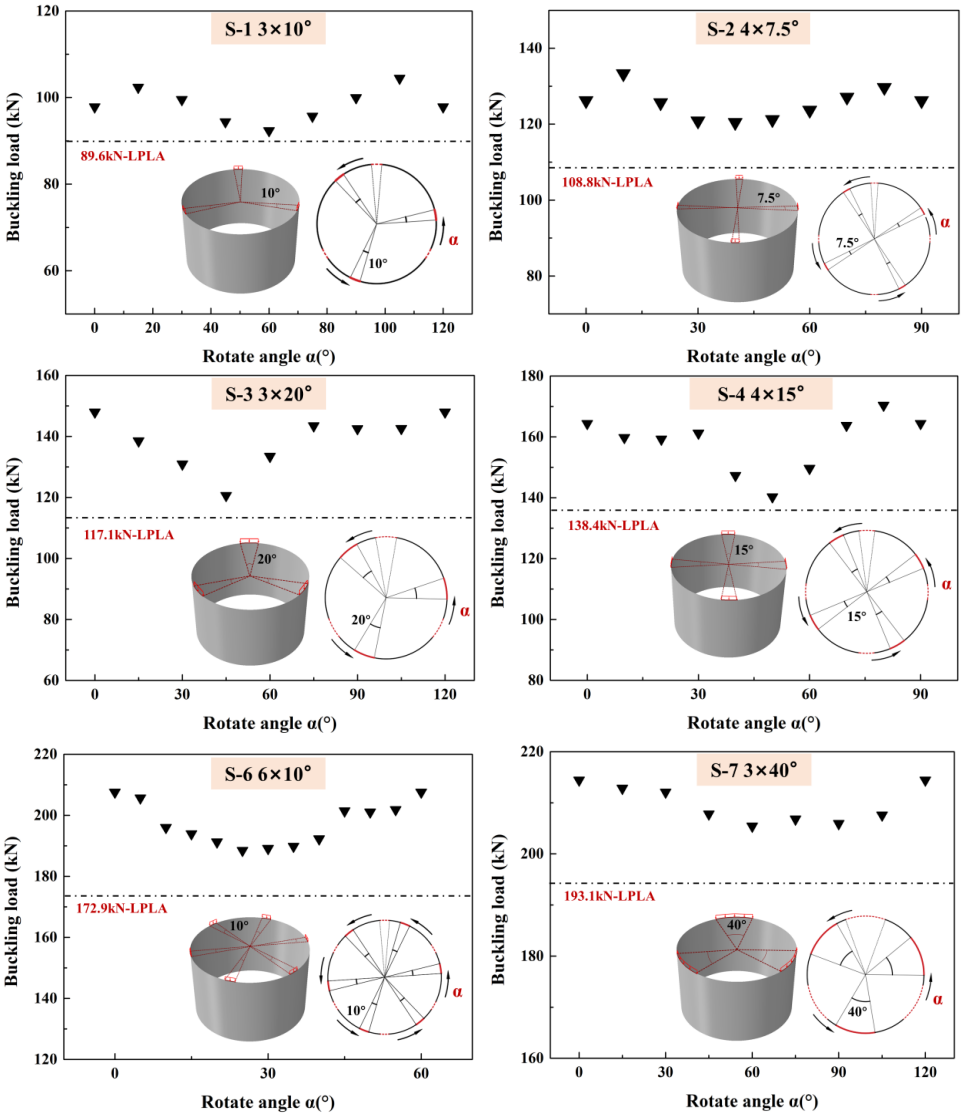


Figure 17. Buckling loads of six cylindrical shells with different imperfection locations and different distributions of partial axial compression loads.

Table 3. Comparison of LPLA results and minimum Num results.

Cylindrical Shell	Loading Region	Num Results (Minimum) (kN)	LPLA Results (kN)	(LPLA-Num)/Num
S-1-A	3 × 10°	92.3	89.6	−2.93%
S-2-A	4 × 7.5°	120.5	108.8	−9.71%
S-3-A	3 × 20°	120.6	117.1	−2.90%
S-4-A	4 × 15°	140.3	138.4	−1.35%
S-6-A	6 × 10°	188.5	172.9	−8.28%
S-7-A	3 × 40°	205.4	193.1	−5.99%

It can be seen from Figure 17 and Table 3 that the change in the relative location of the geometric imperfections to the partial axial compression loads causes a lower buckling load result. Even so, for each cylindrical shell, the LPLA result is lower than all cases of the Num results. This proves that the LPLA can cover the worst effect of imperfections and gives a safe and reliable lower-bound shell buckling load.

3.3. Numerical Studies with Different Shell Dimensions

The shell buckling load results calculated above are all based on cylindrical shells with the same dimensions. It is necessary to examine whether the LPLA can be applied to design steel cylindrical shells of various sizes. The length and thickness of cylindrical shells are, respectively, changed to obtain different radius-to-thickness ratios (R/t) and length-to-radius ratios (L/R). The LPLA results are compared with the numerical simulation results. The measured geometric imperfections are rescaled for application on cylindrical shells with changed dimensions. In addition, four steel cylindrical shell models established by Song et al. [33] are also utilized for comparison. These shells have different types of imperfections and different distributions of partial axial compression loads. The comparison results are shown in Table 4 and Figure 18.

Table 4. Comparison of LPLA results and Num results with different shell dimensions.

Cylindrical Shell	R (mm)	L (mm)	t (mm)	R/t	L/R	Loading Region	Num Results (kN)	LPLA (kN)	(LPLA-Num)/Num
S-2-A	500	530	1.2	417	1.06	7.5° × 4	126.2	108.8	−13.79%
S-2-A1	500	530	1	500	1.06	7.5° × 4	100.2	89.4	−10.78%
S-2-A2	500	530	1.67	300	1.06	7.5° × 4	192.0	153.2	−20.21%
S-2-A3	500	530	2.5	200	1.06	7.5° × 4	314.3	257.4	−18.10%
S-2-A4	500	530	5	100	1.06	7.5° × 4	721.2	603.4	−16.33%
S-6-A	500	530	1.2	417	1.06	10° × 6	207.6	172.9	−16.71%
S-6-A1	500	530	1	500	1.06	10° × 6	166.4	139.8	−15.99%
S-6-A2	500	530	1.67	300	1.06	10° × 6	307.5	244.5	−20.49%
S-6-A3	500	530	2.5	200	1.06	10° × 6	492.2	397.7	−19.20%
S-6-A4	500	530	5	100	1.06	10° × 6	1123.4	958.8	−14.65%
S-2-B1	500	500	1.2	417	1.0	7.5° × 4	119.5	109.1	−8.70%
S-2-B2	500	1000	1.2	417	2.0	7.5° × 4	113.6	105.0	−7.57%
S-2-B3	500	1500	1.2	417	3.0	7.5° × 4	113.1	103.9	−8.13%
S-2-B4	500	250	1.2	417	0.5	7.5° × 4	122.6	109.7	−10.52%
S-6-B1	500	500	1.2	417	1.0	10° × 6	190.5	173.2	−9.08%
S-6-B2	500	1000	1.2	417	2.0	10° × 6	183.1	163.0	−10.98%
S-6-B3	500	1500	1.2	417	3.0	10° × 6	183.3	158.6	−13.48%
S-6-B4	500	250	1.2	417	0.5	10° × 6	195.0	172.8	−11.38%
C-1	500	1500	1	500	3.0	5° × 2	18.8	13.4	−28.72%
C-2	500	1500	1	500	3.0	5° × 2	15.1	13.4	−11.26%
C-3	500	1500	1	500	3.0	30° × 2	40.6	28.9	−28.82%
C-4	500	1500	1	200	3.0	30° × 2	30.1	28.9	−3.99%

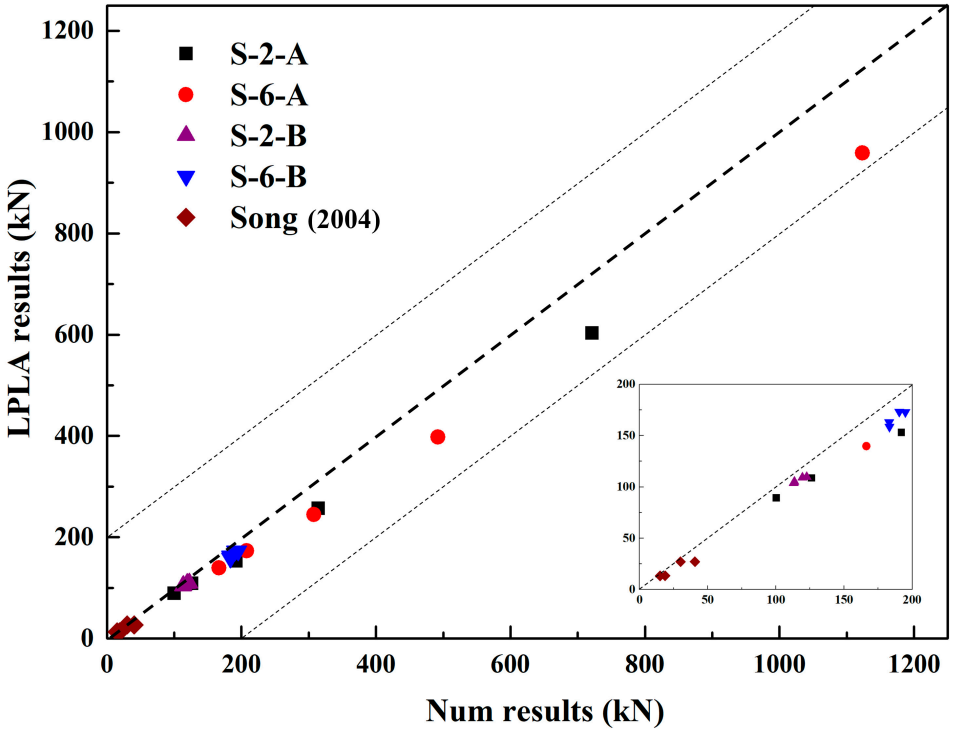


Figure 18. Comparison of LPLA results and Num results with different dimensions, data from [33].

From the comparison results, it can be found that the LPLA can be applied to obtain safe lower-bound buckling loads for cylindrical shells with 100–500 R/t and 0.5–3 L/R. Within this range of shell dimensions, the localized perturbation load approach is proven to be a safe and reliable design method for steel cylindrical shells under partial axial compression.

4. Conclusions

In this paper, the localized perturbation load approach (LPLA) is proposed to achieve the lower-bound buckling loads of thin-walled steel cylindrical shells under partial axial compression. The procedure for the application of the LPLA is provided, and the location and number of perturbation loads are determined by considering the buckling failure mode and imperfection sensitivity of cylindrical shells. Finally, the LPLA is validated via a series of comparison studies. The following conclusions can be drawn.

(1) When the distribution scope of the partial axial compression loads is small, the failure mode of the cylindrical shell is local buckling. The distribution of the partial axial loads causes discrepancies in the load-carrying capacity at different locations in the shell. The shell areas directly below the loading regions have the "weakest" load-carrying capacity. Therefore, applying the perturbation loads on these areas can reflect the influence of imperfections to the greatest extent.

(2) The appropriate number and location of perturbation loads in the LPLA are determined by finite element analysis. One perturbation load is applied right below the middle of each loading region of partial axial compression. The vertical distance between the application points of perturbation loads and the axial loading regions is 0.2 times the shell length.

(3) The results of the LPLA are lower than the test results in all studied loading conditions. In addition, the shell buckling loads under different imperfection locations and various dimensions are all greater than the corresponding lower-bound buckling loads calculated by the LPLA. It is proven that the LPLA can provide rational and conservative lower-bound buckling loads for thin-walled cylindrical shells under partial axial compression. Therefore, the LPLA can be regarded as an appropriate design method for the partially axially compressed steel cylindrical shells in actual engineering.

The application of the LPLA is verified for steel cylindrical shells with the R/t and L/R ratios of 100~500 and 0.5~3, respectively. Future work will include follow-up experimental and numerical studies to validate shells with a wider range of dimensions and shells produced from other materials.

Author Contributions: Conceptualization, H.M. and P.J.; methodology, H.M.; software, H.M. and X.L.; validation, H.M., P.J. and H.X.; investigation, H.M. and Z.C.; writing—original draft preparation, H.M.; writing—review and editing, H.M. and P.J.; visualization, X.L. and H.X.; supervision, P.J.; project administration, P.J.; funding acquisition, P.J. and Z.C. All authors have read and agreed to the published version of the manuscript.

Funding: This research was funded by the National Natural Science Foundation of China (52275163) and the China Postdoctoral Science Foundation (2022M712728).

Data Availability Statement: The data used to support the findings of this study are available from the corresponding author upon request.

Conflicts of Interest: The authors declare no conflict of interest.

References

1. Ni, Y.; Tong, Z.; Rong, D.; Zhou, Z.; Xu, X. Accurate Thermal Buckling Analysis of Functionally Graded Orthotropic Cylindrical Shells under the Symplectic Framework. *Thin-Walled Struct.* **2018**, *129*, 1–9. [CrossRef]
2. Kang, S.-Y.; Won, D.; Park, J.-S.; Kang, Y.-J.; Kim, S. Structural Behavior of Large-Diameter Cylindrical Shell with Stiffened Opening. *Metals* **2021**, *11*, 1413. [CrossRef]
3. Mehta, B.; Hryha, E.; Nyborg, L.; Tholence, F.; Johansson, E. Effect of Surface Sandblasting and Turning on Compressive Strength of Thin 316L Stainless Steel Shells Produced by Laser Powder Bed Fusion. *Metals* **2021**, *11*, 1070. [CrossRef]
4. Jiao, P.; Chen, Z.; Ma, H.; Miao, H.; Ou, H. Buckling Behavior Analysis of Thin-Walled Cylindrical Shell Structure Under Localized Axial Compression Load Based on Initial Imperfection Sensitivity. *Int. J. Str. Stab. Dyn.* **2023**, *2023*, 2350197. [CrossRef]
5. Ma, X.; Hao, P.; Wu, H.; Bo, W.; Bi, X.; Du, K.; Ke, X. High-Fidelity Numerical Simulation and Experimental Validation of a 1600-Mm-Diameter Axial Loaded Grid Stiffened Cylindrical Shell. *Int. J. Solids Struct.* **2023**, *273*, 112262. [CrossRef]
6. Meftah, S.A.; Tounsi, A.; Van Vinh, P. Formulation of Two Nodes Finite Element Model for Geometric Nonlinear Analysis of RHS Beams Accounting for Distortion and Shear Deformations. *Int. J. Steel Struct.* **2022**, *22*, 940–957. [CrossRef]
7. Wagner, H.N.R.; Huehne, C.; Rohwer, K.; Niemann, S.; Wiedemann, M. Stimulating the Realistic Worst Case Buckling Scenario of Axially Compressed Unstiffened Cylindrical Composite Shells. *Compos. Struct.* **2017**, *160*, 1095–1104. [CrossRef]
8. dos Santos, R.R.; Castro, S.G.P. Lightweight Design of Variable-Stiffness Cylinders with Reduced Imperfection Sensitivity Enabled by Continuous Tow Shearing and Machine Learning. *Materials* **2022**, *15*, 4117. [CrossRef]
9. Koiter, W.T. *The Stability of Elastic Equilibrium*; Delft University of Technology: Delft, The Netherlands, 1945.
10. Li, S.-C.; Zhang, Y.-C.; Chang, L.; Zhou, C.-Y.; He, X.-H. Research on Buckling Load of Cylindrical Shell with an Inclined through Crack under External Pressure and Its Solution. *Metals* **2023**, *13*, 174. [CrossRef]
11. Calladine, C. Understanding Imperfection-Sensitivity in the Buckling of Thin-Walled Shells. *Thin-Walled Struct.* **1995**, *23*, 215–235. [CrossRef]
12. Peterson, J.P.; Seide, P.; Weingarten, V.I. *Buckling of Thin-Walled Circular Cylinders—NASA SP-8007*; NASA Space Vehicle Design Criteria; NASA: Washington, DC, USA, 1968.
13. Cooley, S.A.; Yang, H.; Virgin, L.N. 3D-Printing and Cylinder Buckling: Challenges and Opportunities. *Proc. R. Soc. A-Math. Phys. Eng. Sci.* **2023**, *381*, 20220035. [CrossRef] [PubMed]
14. Castro, S.G.P.; Zimmermann, R.; Arbelo, M.A.; Degenhardt, R. Exploring the Constancy of the Global Buckling Load after a Critical Geometric Imperfection Level in Thin-Walled Cylindrical Shells for Less Conservative Knock-down Factors. *Thin-Walled Struct.* **2013**, *72*, 76–87. [CrossRef]
15. Wagner, H.N.R.; Hühne, C.; Elishakoff, I. Probabilistic and Deterministic Lower-Bound Design Benchmarks for Cylindrical Shells under Axial Compression. *Thin-Walled Struct.* **2020**, *146*, 106451. [CrossRef]
16. Arbocz, J.; Babcock, C.D. Prediction of Buckling Loads Based on Experimentally Measured Initial Imperfections. In *Buckling of Structures*; Budiansky, B., Ed.; Springer: Berlin/Heidelberg, Germany, 1976; pp. 291–311. ISBN 978-3-642-50994-0.
17. Winterstetter, T.A.; Schmidt, H. Stability of Circular Cylindrical Steel Shells under Combined Loading. *Thin-Walled Struct.* **2002**, *40*, 893–909. [CrossRef]
18. Huehne, C.; Rolfes, R.; Breitbach, E.; Tessmer, J. Robust Design of Composite Cylindrical Shells under Axial Compression—Simulation and Validation. *Thin-Walled Struct.* **2008**, *46*, 947–962. [CrossRef]
19. Hao, P.; Wang, B.; Du, K.; Li, G.; Tian, K.; Sun, Y.; Ma, Y. Imperfection-Insensitive Design of Stiffened Conical Shells Based on Equivalent Multiple Perturbation Load Approach. *Compos. Struct.* **2016**, *136*, 405–413. [CrossRef]
20. Wagner, H.N.R.; Huehne, C.; Niemann, S.; Khakimova, R. Robust Design Criterion for Axially Loaded Cylindrical Shells—Simulation and Validation. *Thin-Walled Struct.* **2017**, *115*, 154–162. [CrossRef]

21. Arbelo, M.A.; Castro, S.G.; Kalnins, K.; Ozolins, O.; Khakimova, R.; Degenhardt, R. Experimental Characterization of Buckling Load on Imperfect Cylindrical Shells Using the Multiple Perturbation Load Approach. In Proceedings of the 13th European Conference on Spacecraft Structures, Materials and Environmental Testing, Braunschweig, Germany, 1–4 April 2014; Volume 727.
22. Jiao, P.; Chen, Z.; Tang, X.; Su, W.; Wu, J. Design of Axially Loaded Isotropic Cylindrical Shells Using Multiple Perturbation Load Approach—Simulation and Validation. *Thin-Walled Struct.* **2018**, *133*, 1–16. [CrossRef]
23. Arbelo, M.A.; Degenhardt, R.; Castro, S.G.P.; Zimmermann, R. Numerical Characterization of Imperfection Sensitive Composite Structures. *Compos. Struct.* **2014**, *108*, 295–303. [CrossRef]
24. Asmolovskiy, N.; Tkachuk, A.; Bischoff, M. Numerical Approaches to Stability Analysis of Cylindrical Composite Shells Based on Load Imperfections. *Eng. Comput.* **2015**, *32*, 498–518. [CrossRef]
25. Hao, P.; Wang, B.; Li, G.; Meng, Z.; Tian, K.; Zeng, D.; Tang, X. Worst Multiple Perturbation Load Approach of Stiffened Shells with and without Cutouts for Improved Knockdown Factors. *Thin-Walled Struct.* **2014**, *82*, 321–330. [CrossRef]
26. Wang, B.; Hao, P.; Li, G.; Fang, Y.; Wang, X.; Zhang, X. Determination of Realistic Worst Imperfection for Cylindrical Shells Using Surrogate Model. *Struct. Multidiscip. Optim.* **2013**, *48*, 777–794. [CrossRef]
27. Tian, K.; Wang, B.; Hao, P.; Waas, A.M. A High-Fidelity Approximate Model for Determining Lower-Bound Buckling Loads for Stiffened Shells. *Int. J. Solids Struct.* **2018**, *148*, 14–23. [CrossRef]
28. Ma, W.; Sun, Z.; Wu, H.; Xu, L.; Zeng, Y.; Wang, Y.; Huang, G. Buckling Analysis of Thin-Walled Circular Shells under Local Axial Compression Using Vector Form Intrinsic Finite Element Method. *Metals* **2023**, *13*, 564. [CrossRef]
29. Yang, L.; Qiu, T.; Dong, Y. Buckling Analysis of Cylindrical Shells with Variable Thickness Subjected to Non-Uniform Axial Compression by Establishing a Novel Quadratic Perturbation Technique. *Int. J. Struct. Stab. Dyn.* **2022**, *22*, 2250120. [CrossRef]
30. Wang, P.; Zhu, X.; Liu, M.; Li, Y. Buckling Behaviors and Simplified Design Method for Steel Silos under Locally Distributed Axial Load. *J. Constr. Steel. Res.* **2017**, *134*, 114–134. [CrossRef]
31. Jiao, P.; Chen, Z.; Ma, H.; Zhang, D.; Wu, J.; Ge, P.; Gu, Y. Buckling Test of Thin-Walled Metallic Cylindrical Shells under Locally Distributed Axial Compression Loads. In Proceedings of the Pressure Vessels and Piping Conference, Online, 3 August 2020; American Society of Mechanical Engineers: Amsterdam, The Netherlands, 2020; Volume 83839, p. V003T03A067.
32. Rotter, J.M.; Cai, M.; Holst, J.M.F.G. Buckling of Thin Cylindrical Shells Under Locally Elevated Compressive Stresses. *J. Press. Vessel Technol.-Trans. ASME* **2011**, *133*, 011204. [CrossRef]
33. Song, C.Y.; Teng, J.G.; Rotter, J.M. Imperfection Sensitivity of Thin Elastic Cylindrical Shells Subject to Partial Axial Compression. *Int. J. Solids Struct.* **2004**, *41*, 7155–7180. [CrossRef]
34. Khelil, A. Buckling of Steel Shells Subjected to Non-Uniform Axial and Pressure Loading. *Thin-Walled Struct.* **2002**, *40*, 955–970. [CrossRef]
35. Dey, T.; Ramachandra, L.S. Dynamic Stability of Simply Supported Composite Cylindrical Shells under Partial Axial Loading. *J. Sound Vibr.* **2015**, *353*, 272–291. [CrossRef]
36. Jiao, P.; Chen, Z.; Ma, H.; Ge, P.; Gu, Y.; Miao, H. Buckling Behaviors of Thin-Walled Cylindrical Shells under Localized Axial Compression Loads, Part 1: Experimental Study. *Thin-Walled Struct.* **2021**, *166*, 108118. [CrossRef]
37. Jiao, P.; Chen, Z.; Ma, H.; Ge, P.; Gu, Y.; Miao, H. Buckling Behaviors of Thin-Walled Cylindrical Shells under Localized Axial Compression Loads, Part 2: Numerical Study. *Thin-Walled Struct.* **2021**, *169*, 108330. [CrossRef]
38. Ma, H.; Jiao, P.; Li, H.; Cheng, Z.; Chen, Z. Buckling Analyses of Thin-Walled Cylindrical Shells Subjected to Multi-Region Localized Axial Compression: Experimental and Numerical Study. *Thin-Walled Struct.* **2023**, *183*, 110330. [CrossRef]
39. Castro, S.G.P.; Zimmermann, R.; Arbelo, M.A.; Khakimova, R.; Hilburger, M.W.; Degenhardt, R. Geometric Imperfections and Lower-Bound Methods Used to Calculate Knock-down Factors for Axially Compressed Composite Cylindrical Shells. *Thin-Walled Struct.* **2014**, *74*, 118–132. [CrossRef]

Disclaimer/Publisher's Note: The statements, opinions and data contained in all publications are solely those of the individual author(s) and contributor(s) and not of MDPI and/or the editor(s). MDPI and/or the editor(s) disclaim responsibility for any injury to people or property resulting from any ideas, methods, instructions or products referred to in the content.